

1854. Investigation on the aerodynamic characteristics of a rocket-target for the system “Stinger”

Algimantas Fedaravičius¹, Sigitas Kilikevičius², Arvydas Survila³

Kaunas University of Technology, Kaunas, Lithuania

¹Corresponding author

E-mail: ¹algimantas.fedaravicius@ktu.lt, ²sigitas.kilikevicius@ktu.lt, ³arvydas.survila@ktu.lt

(Received 27 June 2015; received in revised form 3 August 2015; accepted 11 August 2015)

Abstract. This paper deals with the aerodynamic simulation and external ballistics calculation which were required for developing a rocket-target for the system “Stinger” in order to identify an optimal configuration of a nose shape. Airflow around several rockets with different nose shapes is investigated in this paper. The mathematical background of the computational fluid dynamics techniques applied for the investigation is presented and a computational model of airflow around the rockets is developed using ANSYS CFX software. Pressure contours, airflow streamlines, drag force and drag coefficient dependencies on the rocket’s velocity are presented. Considering the results, the most suitable nose shape for the rocket-target is selected.

Keywords: airflow, drag force, drag coefficient, rocket-target.

1. Introduction

The geometrical and design parameters and the exterior ballistics characteristics of a rocket are usually estimated for a particular rocket design. The range of rocket’s velocities can be rather wide. The present design required developing a rocket-target for the system “Stinger” which is 5 meters in length and 0.4 meters in diameter, at a velocity range below 250 m/s. Several possible nose shapes are suitable in this case, such as various ogive, conical or elliptical shapes [1, 2]. It is known that various aerodynamic characteristics have a great influence on the exterior ballistics of the rocket, however, the drag force and drag coefficient are the most important parameters necessary for the investigation of exterior ballistics.

Computational fluid dynamic (CFD) techniques to calculate the aerodynamic coefficients of many complex geometry and complex flow phenomena were recently demonstrated [3, 4]. CFD is suitable to use at conceptual design stage of the aerodynamic configurations as it is able to get aerodynamic characteristics from more configurations than wind tunnel testing. Therefore, CFD methods are widely used in order to predict aerodynamic characteristics of rockets during various development stages [5-7].

The main objective of this paper is to identify an optimal configuration of a nose shape by a CFD simulation.

2. Mathematical background of flow simulation

The airflow around the rocket was modeled using the commercial finite element software ANSYS CFX. The set of equations solved by ANSYS CFX are the Reynolds averaged equations given below [8].

$$\frac{\partial \rho}{\partial t} + \frac{\partial}{\partial x_j} (\rho U_j) = 0, \quad (1)$$

$$\frac{\partial \rho U_i}{\partial t} + \frac{\partial}{\partial x_j} (\rho U_i U_j) = -\frac{\partial p}{\partial x_i} + \frac{\partial p}{\partial x_j} (\tau_{ij} - \rho \overline{u_i u_j}) + S_M, \quad (2)$$

where ρ is the density, U is the vector of velocity, p is the pressure, S_M is the momentum source, τ is the molecular stress tensor (including both normal and shear components of the stress) and $\rho \overline{u_i u_j}$ are the Reynolds stresses.

The Reynolds stresses need to be modeled by additional equations of known quantities in order to achieve "closure". The equations used to close the system define the type of turbulence model [8].

In this study the shear stress transport (SST) turbulence model was applied which is the most suitable for aeronautics flows with strong adverse pressure gradients and separation. The model (written in conservation form) is given by the following [9]:

$$\frac{\partial(\rho k)}{\partial t} + \frac{\partial(\rho U_i k)}{\partial x_i} = \tilde{P}_k - \beta^* \rho k \omega + \frac{\partial}{\partial x_i} \left[(\mu + \sigma_k \mu_t) \frac{\partial k}{\partial x_i} \right], \quad (3)$$

$$\begin{aligned} \frac{\partial(\rho \omega)}{\partial t} + \frac{\partial(\rho U_i \omega)}{\partial x_i} &= \alpha \rho S^2 - \beta \rho \omega^2 + \frac{\partial}{\partial x_i} \left[(\mu + \sigma_\omega \mu_t) \frac{\partial \omega}{\partial x_i} \right] \\ &+ 2(1 - F_1) \rho \sigma_{\omega 2} \frac{1}{\omega} \frac{\partial k}{\partial x_i} \frac{\partial \omega}{\partial x_i}, \end{aligned} \quad (4)$$

where k is the turbulence kinetic energy, ω is the turbulence frequency, μ_t is the turbulent viscosity. Blending function F_1 is defined by:

$$F_1 = \tanh \left\{ \left\{ \min \left[\max \left(\frac{\sqrt{k}}{\beta^* \omega y}, \frac{500\nu}{y^2 \omega} \right), \frac{4\rho\sigma_{\omega 2} k}{CD_{k\omega} y^2} \right] \right\}^4 \right\}, \quad (5)$$

where y is the distance from the field point to the nearest wall:

$$CD_{k\omega} = \max \left(2\rho\sigma_{\omega 2} \frac{1}{\omega} \frac{\partial k}{\partial x_i} \frac{\partial \omega}{\partial x_i}, 10^{-10} \right). \quad (6)$$

F_1 is equal to zero away from the surface (k - ε model), and switches over to one inside the boundary layer (k - ω model).

The turbulent eddy viscosity is defined as follows:

$$v_t = \frac{a_1 k}{\max(a_1 \omega, S F_2)}, \quad (7)$$

where $v_t = \mu_y / \rho$, S is the invariant measure of the strain rate and F_2 is a second blending function:

$$F_2 = \tanh \left\{ \left[\max \left(\frac{2\sqrt{k}}{\beta^* \omega y}, \frac{500\nu}{y^2 \omega} \right) \right]^2 \right\}. \quad (8)$$

A production limiter is used in the SST model to prevent the build-up of turbulence in stagnation regions:

$$P_k = \mu_t \frac{\partial U_i}{\partial x_j} \left(\frac{\partial U_i}{\partial x_j} + \frac{\partial U_j}{\partial x_i} \right) \rightarrow \tilde{P}_k = \min(P_k, 10 \cdot \beta^* \rho k \omega). \quad (9)$$

The constants for the SST model are: $a_1 = 0.31$, $\beta^* = 0.09$, $\alpha_1 = 5/9$, $\beta_1 = 3/40$, $\sigma_{k1} = 0.85$, $\sigma_{\omega 1} = 0.5$, $\alpha_2 = 0.44$, $\beta_2 = 0.0828$, $\sigma_{k2} = 1$, $\sigma_{\omega 2} = 0.856$.

The total energy heat transfer model was used in this study which models the transport of enthalpy and includes kinetic energy effects. The total energy equation [8]:

$$\frac{\partial(\rho h_{tot})}{\partial t} - \frac{\partial p}{t} + \nabla \cdot (\rho U h_{tot}) = \nabla(\lambda \nabla T) + \nabla \cdot (U \cdot \tau) + U \cdot S_M + S_E, \quad (10)$$

where λ is thermal conductivity, T is temperature, S_E is the energy source h_{tot} is the total enthalpy, related to the static enthalpy $h(T, p)$ by:

$$h_{tot} = h + \frac{1}{2} U^2. \tag{11}$$

3. Computational model of the airflow simulation

Several possible nose shapes (ogive, conical, 0.5 power and elliptical) for the rocket-target were investigated in respect of aerodynamic characteristics (Fig. 1). The overall dimensions of the rocket are 0.4 m in diameter and 5.6 m in length and the overall dimension between the fins is 1.2 m. The length of the nose is 0.4 m (the same for all the configurations).

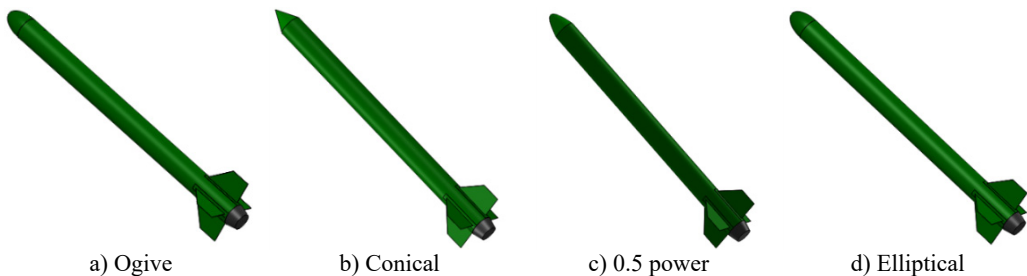


Fig. 1. Rockets with different shape nose cones

Three dimensional models of computational domains for the rockets were produced in SolidWorks and imported into ANSYS CFX. Computational numerical finite element models for a numerical simulation of airflow around the rockets were generated in ANSYS CFX software. Only a half of each model is discretized with a symmetry boundary condition in order to save computational time. A rectangular fluid domain was placed around the rocket, in order to limit the fluid domain where the CFD simulation is carried out. The limit upstream the body was located at a distance of 3 rocket's lengths and the limit downstream the body was located at a distance of 5 rocket's lengths, whereas the lateral boundaries were placed at a distance of about 35 diameters (~ 2.5 rocket's lengths).

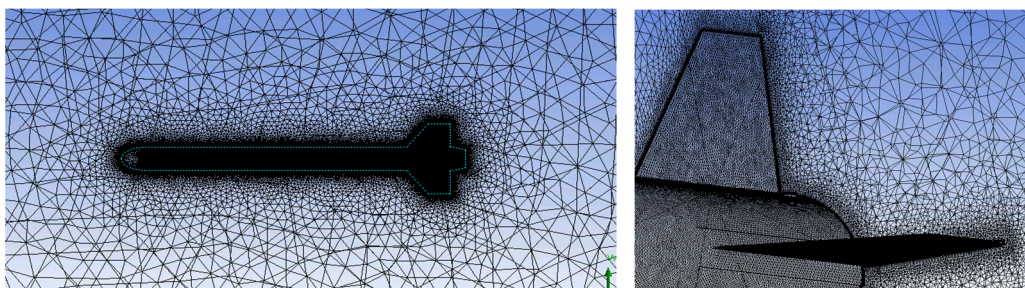


Fig. 2. Computational grid cuts at different locations

An unstructured computational grid was generated inside this fluid volume. The grid is of hybrid type, i.e. made up of prismatic elements in the viscous region located in close proximity of the body, whereas tetrahedral elements were used to fill the remaining fluid volume. After a mesh sensitivity analysis, the maximum size of tetrahedral elements in the grid was set to 13.5 mm and the minimum size was 7.5 mm. 20 layers of prism elements were created on the surface of the rocket with the maximum thickness of 15 mm and the growth rate 1.2. On the surface of the rocket the grid was made distinctly denser, the size of prism elements was set to 3.75 mm. The grid contains an overall size of ~ 7.18 million elements including ~ 3.5 million prism elements (Fig. 2).

The assigned range of velocity was between 0.3 and 0.8 Mach number. The standard atmosphere values of all the other thermodynamic variables at sea level were used as input flow conditions in the computations, that is a freestream static temperature of 15 °C and a freestream static pressure of 101327 Pa. The surface of the rocket was defined as a non-slippery smooth wall. The outside walls of the computational domain (the lateral boundaries) were defined as free slip walls.

The analysis was carried out considering the compressible formulation of the Navier-Stokes equation system.

4. Results of the airflow simulation

Results of the simulation of the airflow around the rockets were obtained. The pressure distribution at the surface of the rocket and the cross-section plane is presented in Fig. 3. Velocity streamlines for the rockets at 0.8 Mach number are shown in Fig. 4.

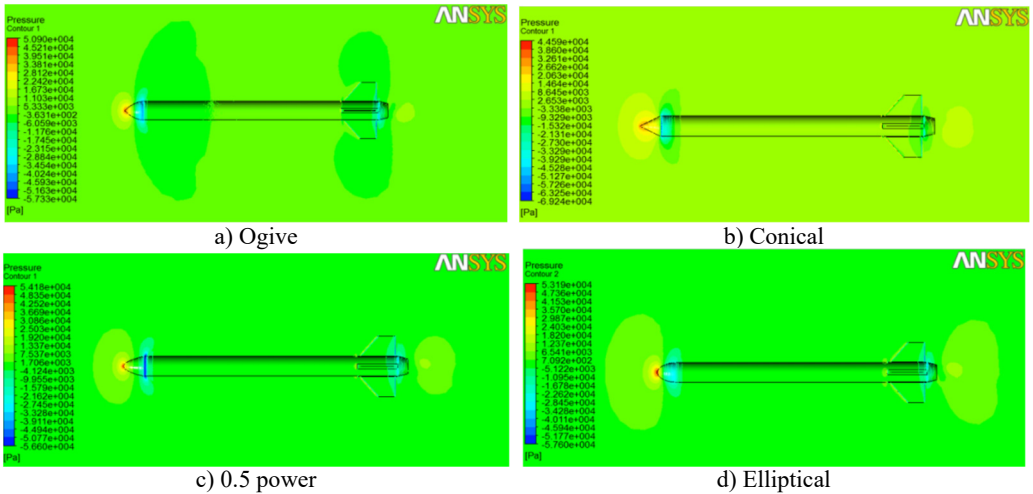


Fig. 3. Pressure on the cross-section plane and the rocket surface, under $M = 0.8$

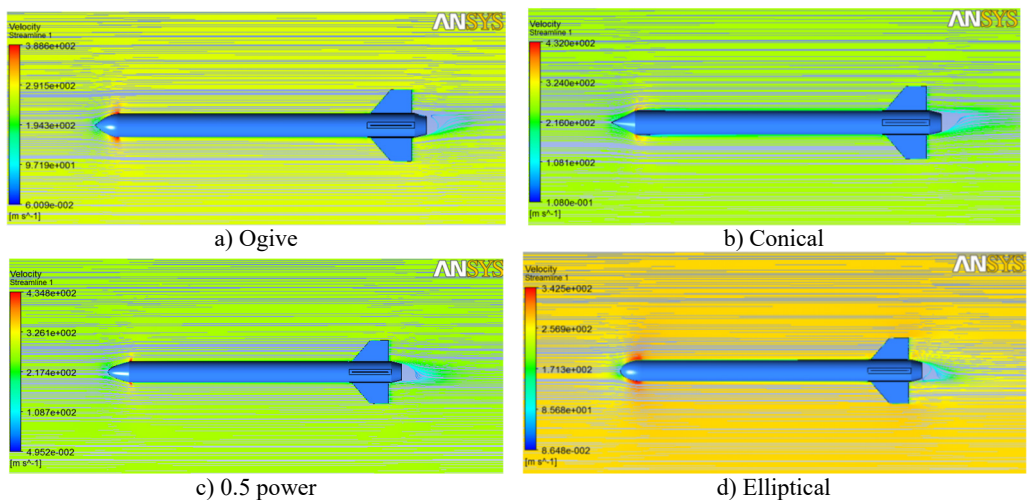


Fig. 4. Velocity streamlines on the cross-section plane, under $M = 0.8$

The drag coefficient of the rockets was calculated by the following expression [10]:

$$C_d = \frac{F_d}{0.5\rho U^2 A} \tag{12}$$

where F_d is the drag force, obtained from the simulation results; ρ is the air density; U is the velocity of airflow; A is the reference area.

Dependences of the drag force on Mach number for different cones of the rockets is shown in Fig. 5. The highest drag force was for the rocket with the conical nose in all velocity ranges. The simulation showed that the drag force of the rocket with the ogive, conical and elliptical nose shapes is very similar. In the range of 0.3...0.6 Mach number, the lowest drag force is with the ogive nose, then follow the 0.5 power nose and the elliptical nose. In the range of 0.6...0.8 Mach number, the lowest drag force is with the elliptical nose, then follow the ogive nose and the 0.5 power nose. Accordingly, these tendencies reflect on the drag coefficient (Fig. 6).

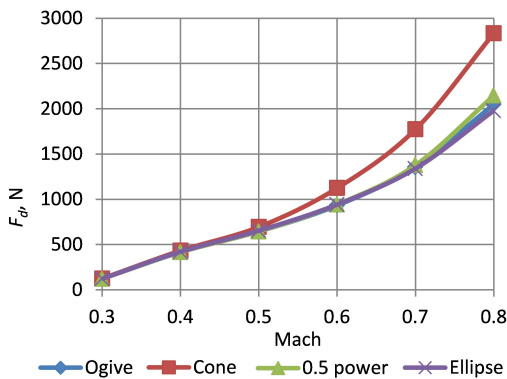


Fig. 5. Dependences of the drag force on Mach number for different cones of the rockets

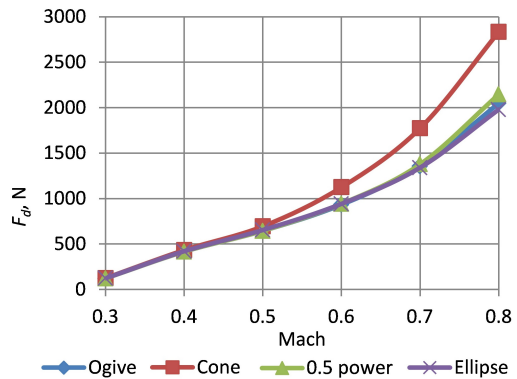


Fig. 6. Dependences of the drag coefficient on Mach number for different cones of the rockets

The drag coefficient of the rocket with the ogive, conical and elliptical nose shapes is very close and, in the range of 0.3...0.6 Mach number, it varies from approximately 0.272 (ogive) to 0.353 (0.5 power). As for the conical nose shape, the drag coefficient varies from 0.286 to 0.466 in the same Mach number range.

Since the elliptical nose shape gives the lowest drag force at 0.8 Mach, this shape was selected for further development of the rocket-target.

5. Conclusions

A simulation of the airflow around rockets with different nose shapes is carried out and pressure contours, airflow streamlines, drag force and drag coefficient dependences on the rocket's velocity are obtained.

The simulation showed that the highest drag force was for the rocket with the conical nose in all velocity ranges. It is seen, that the drag force of the rocket with the ogive, conical and elliptical nose shapes is very similar. In the range of 0.3...0.6 Mach number, the lowest drag force is with the ogive nose, then follow the 0.5 power nose and the elliptical nose. In the range of 0.6...0.8 Mach number, the lowest drag force is with the elliptical nose, then follow the ogive nose and the 0.5 power nose. Accordingly, these tendencies reflect on the drag coefficient.

The drag coefficient of the rocket with the ogive, conical and elliptical nose shapes is very close and, in the range of 0.3...0.6 Mach number, it varies from approximately 0.272 (ogive) to 0.353 (0.5 power). As for the conical nose shape, the drag coefficient varies from 0.286 to 0.466 in the same Mach number range.

Since the elliptical nose shape gives the lowest drag force at 0.8 Mach, this shape was selected for further development of the rocket-target.

References

- [1] Military Design Handbook. Design of Aerodynamically Stabilized Free Rockets. Department of Defense, U.S. Army Missile Command, 1990.
- [2] **Fedaravičius A., Kilikevičius S., Survila A.** Optimization of the rocket's nose and nozzle design parameters in respect to its aerodynamic characteristics. Journal of Vibroengineering, Vol. 14, Issue 3, 2012, p. 1390-1398.
- [3] **Abbas L. K., Chen D., Rui X.** Numerical calculation of effect of elastic deformation on aerodynamic characteristics of a rocket. International Journal of Aerospace Engineering, 2014, p. 478534.
- [4] **Suresha C., Rameshb K., Paramaguruc V.** Aerodynamic performance analysis of a non-planar C-wing using CFD. Aerospace Science and Technology, Vol. 40, 2015, p. 56-61.
- [5] **Kuzuu K., Nonaka S., Aono J., Shima E.** Aerodynamic characteristics and kinematic analysis during turnover of a reusable sounding rocket. 51st AIAA Aerospace Sciences Meeting including the New Horizons Forum and Aerospace Exposition, 2013.
- [6] **Li Y., Reimann B., Eggers T.** Numerical investigations on the aerodynamics of SHEFEX-III launcher. Acta Astronautica, Vol. 97, 2014, p. 99-108.
- [7] **Bartels R. E.** Flexible launch stability analysis using steady and unsteady computational fluid dynamics. Journal of Spacecraft and Rockets, Vol. 49, Issue 4, 2012, p. 644-650.
- [8] ANSYS CFX-Solver Theory Guide. PA 15317, p. 23-96.
- [9] **Menter F. R., Kuntz M., Langtry R.** Ten years of industrial experience with the SST turbulence model. Turbulence, Heat and Mass Transfer 4, Begell House, 2003, p. 625-632.
- [10] **Mills A. F., Irwin R. D.** Basic Heat and Mass Transfer. University of California at Los Angeles, 1995, p. 254-921.



Algimantas Fedaravičius received Dr.Sc. degree in Mechanical Engineering from Kaunas University of Technology, Kaunas, Lithuania in 1979; Dr. Habil. degree in Mechanical Engineering from Kaunas University of Technology in 1988. Now he works at Kaunas University of Technology. His current research interests include dynamics of mechanical systems, vibration analysis, aerodynamics, ballistics and applications.



Sigitas Kilikevičius received Dr.Sc. degree in Mechanical Engineering from Kaunas University of Technology, Kaunas, Lithuania, in 2009. Now he works at Kaunas University of Technology. His current research interests include analysis and simulation of mechanical systems, computational fluid dynamics, vibration analysis and applications.



Arvydas Survila received M.Sc. degree in Electronics Engineering from Kaunas University of Technology, Kaunas, Lithuania, in 1996. Now he works at Kaunas University of Technology. His current research interests include control, vibration analysis, ballistics and applications.